Volume 61
Number 64
18 August 2025
Pages 11869–12044

ChemComm

Chemical Communications

rsc.li/chemcomm

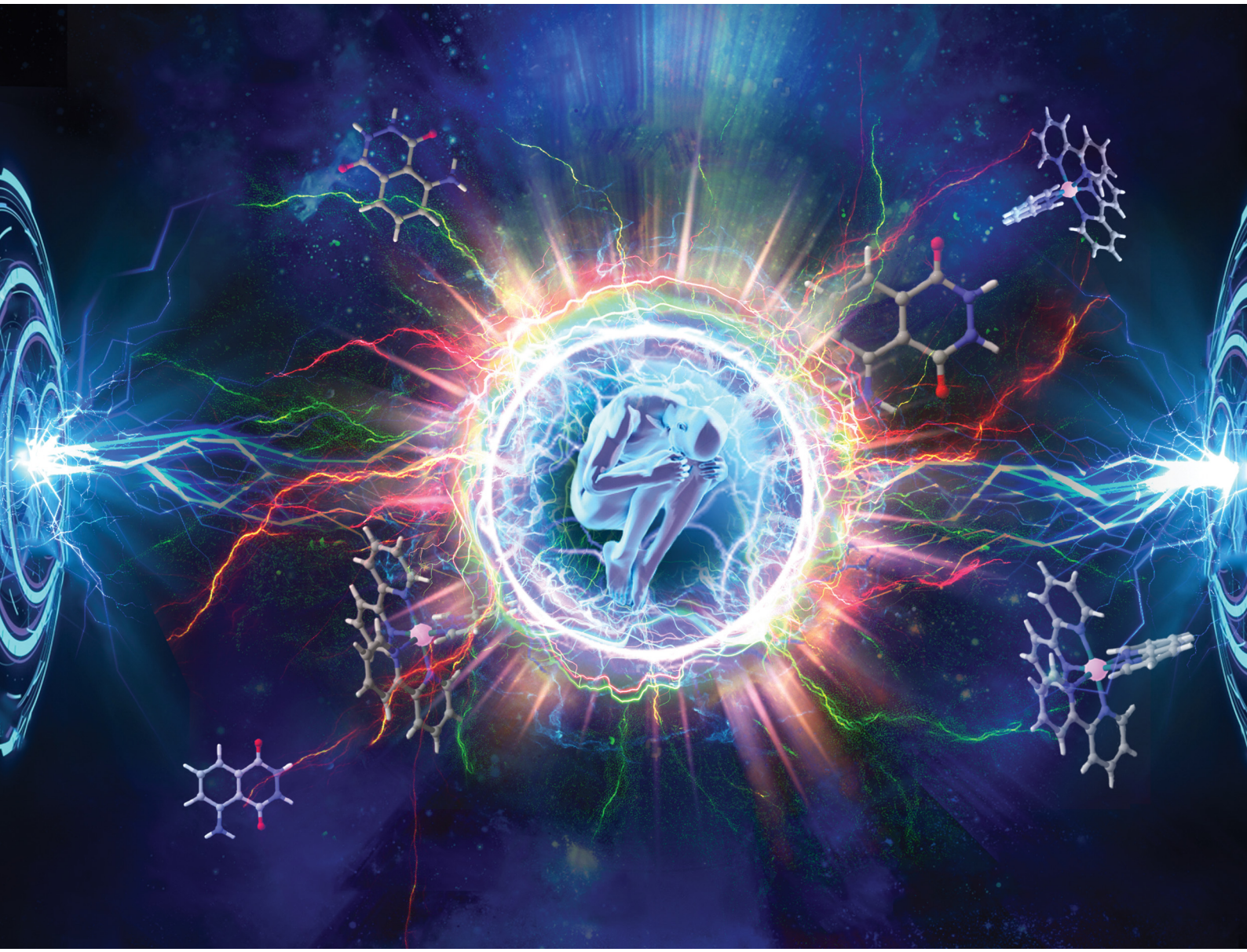

ISSN 1359-7345

ROYAL SOCIETY OF CHEMISTRY

FEATURE ARTICLE

Neso Sojic *et al.*

Bipolar electrochemiluminescence: from fundamentals to emerging trends

ChemComm

ROYAL SOCIETY OF CHEMISTRY

FEATURE ARTICLE

View Article Online
View Journal | View Issue

Cite this: *Chem. Commun.*, 2025, **61**, 11896

Bipolar electrochemiluminescence: from fundamentals to emerging trends

Rui Zou,†[ab] Leslie R. Arias-Aranda,†[b] Gerardo Salinas,[b] Alexander Kuhn,[b] Laurent Bouffier[b] and Neso Sojic*[b]

The combination of electrochemiluminescence (ECL) and bipolar electrochemistry (BE) has advanced the development of a new generation of optical devices, offering new possibilities for high-efficiency detection and sensing applications. ECL, a luminescent phenomenon triggered at the electrode surface and driven by redox reactions, has become a versatile technique for highly sensitive detection. Meanwhile, BE enables the remote activation of electrochemical processes without the need for a direct electric connection to the electrodes, thus simplifying the design and miniaturization of electrochemical systems. The integration of both technologies optimizes the interaction between luminophores and bipolar electrodes, improving the efficiency of analyte detection and facilitating the implementation of parallel or multiplexed detection strategies, thus increasing precision and repeatability. This synergy has extended the application scope in areas such as bioanalysis, environmental analysis, and pollutant detection. This review analyzes the fundamental principles of ECL and BE, as well as their synergy in advanced systems, covering the design of spatially confined structures that improve the polarization of bipolar electrodes, thus reducing the threshold energy required to activate ECL and enhancing its efficiency. Additionally, the incorporation of dynamic elements, such as rotating electrodes and microfluidic platforms, has facilitated real-time analysis and the visualization of electrochemical processes at both macroscopic and microscopic levels. The combination of ECL and BE technologies has not only expanded diagnostic and monitoring possibilities in autonomous systems, but has also paved the way for the development of the next generation of analytical technologies, with a significant impact on various scientific challenges.

Received 19th May 2025,
Accepted 7th July 2025

DOI: 10.1039/d5cc02825f

rsc.li/chemcomm

[a] *Ningxia Key Laboratory of Green Catalytic Materials and Technology, College of Chemistry and Chemical Engineering, Ningxia Normal University, China*
[b] *Univ. Bordeaux, Bordeaux INP, ISM, UMR 5255 CNRS, Site ENSMAC, 33607 Pessac, France. E-mail: sojic@u-bordeaux.fr*
† Rui Zou and Leslie R. Arias-Aranda contributed equally.

Rui Zou

Rui Zou is a full associated professor at the College of Chemistry and Chemical Engineering, Ningxia Normal University. She received her PhD degree from Beijing University of Chemical Technology in 2022. Her research activities focus on electrochemiluminescence, electrochemical sensors and characterization of nanomaterials.

Leslie R. Arias-Aranda

Leslie R. Arias-Aranda holds a BSc and an MSc degree in Chemistry from the National Autonomous University of Mexico (UNAM). She is currently pursuing her PhD at the Institute of Molecular Sciences (ISM) at the University of Bordeaux, France, within the Analytical Nanosystems group (NSYSA), under the supervision of Dr. Laurent Bouffier and Prof. Neso Sojic. Her research focuses on analytical electrochemistry, with particular emphasis on electrochemiluminescence and bipolar electrochemistry.

Introduction

Electrochemiluminescence (ECL) is a well-known physicochemical phenomenon in which light is generated after highly exergonic electron transfer reactions that take place at the surface of an electrode.[1–4] This in turn generates the excited state of a luminophore, which emits light upon radiative relaxation. Due to its high sensitivity and spatial resolution, combined with its low signal-to-noise ratio, ECL has evolved from a laboratory curiosity to an everyday tool in multiple applications from bioanalysis to imaging.[5–16] From a molecular point of view, ECL can be generated following either the annihilation or the co-reactant pathway. In the former case, the oxidized and reduced forms of the luminophore are generated alternately and react together producing its excited state. In contrast, for the co-reactant pathway, a sacrificial reagent undergoes an irreversible electron transfer producing highly reactive redox species. These short-lived species react with either the oxidized or the reduced form of the luminophore, producing once again its excited state. Among the different luminophore/co-reactant systems, tris(2,2′-bipyridine)ruthenium(II)/tri-*n*-propylamine ($[Ru(bpy)_3]^{2+}$/TPrA) and luminol/H_2O_2 systems stand out due to their high ECL efficiency.[3,17] Although countless ECL-based approaches have been designed, the large majority are powered by conventional electrochemistry. In particular, the working electrode requires a direct connection to a power source, which can limit its use, especially for *in situ* or *in vivo* applications. Thus, the development of wireless ECL systems is highly desired.

In this context, bipolar electrochemistry (BE) has emerged as an interesting alternative to conventional electrochemistry. BE is achieved in a wireless manner, promoting asymmetric reactivity on conducting objects, or so-called bipolar electrodes (BPEs).[18–29] Briefly, by coupling thermodynamically spontaneous redox reactions ($\Delta_r G < 0$) or in the presence of a high enough external electric field (ε) ($\Delta_r G > 0$), a polarization

Gerardo Salinas

Gerardo Salinas received his Master's and PhD degrees in electrochemistry from the National Autonomous University of Mexico (UNAM). Since 2018, he has been performing postdoctoral studies at the Institute of Molecular Sciences (ISM) at the University of Bordeaux (France) under the supervision of Prof. Alexander Kuhn. His research interests include bipolar electrochemistry, conducting polymers, electrochemistry-based light emitting devices and magneto-electrochemistry.

Alexander Kuhn

Alexander Kuhn obtained his Master's degree in chemistry from TU Munich and his PhD from the University of Bordeaux. After his post-doc research at Caltech, he moved back to Bordeaux where he is currently a Full Professor in chemistry. He is also an Adjunct Professor at VISTEC, Thailand, a Distinguished Professor at Henan University, China, a senior member of the Institut Universitaire de France, a distinguished senior member of the French Chemical Society and a Fellow of the International Society of Electrochemistry. He is the recipient of several honors, including the Grand Prix Süe of the French Chemical Society and the science medal in silver of the CNRS.

Laurent Bouffier

Laurent Bouffier graduated from the University of Grenoble in France where he also obtained his PhD in organic chemistry in 2005. He moved to the University of Liverpool in the UK as a postdoctoral research associate in physical chemistry and materials science. He was appointed by the CNRS (Centre National de la Recherche Scientifique) in 2010. He is affiliated to the Institute of Molecular Sciences (ISM) at the University of Bordeaux in France. His research activities focus on bipolar electrochemistry, electrogenerated chemiluminescence and in situ microscopy.

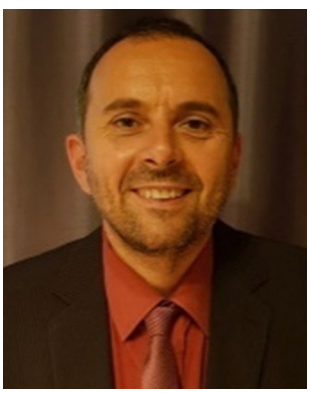

Neso Sojic

Neso Sojic is a professor in the Institut des Sciences Moléculaires (University of Bordeaux, Bordeaux INP, CNRS). He received his PhD in electrochemistry from the Université Pierre et Marie Curie (Paris, France). After postdoctoral studies at the University of Texas at Dallas, he joined the faculty at the University of Bordeaux (France). His main research interests are in analytical electrochemistry, electrochemiluminescence, bioelectrochemistry, microscopy and fiber optic sensors.

potential difference (ΔV) is induced across the BPE.[30] When ΔV overcomes the thermodynamic threshold potential (ΔV_{min}), established for a set of electroactive species, redox reactions take place at each extremity of the BPE. Due to its different advantages, such as its wireless nature, the tuning of the asymmetric electrochemical activity and the possible use of BE arrays, BE has gained considerable attention in multiple fields such as electrosynthesis, sensing, materials science and environmental remediation.[31–37] Thus, the synergetic effect between BE and ECL has stimulated the development of multiple wireless light-emitting platforms.[38,39] In this feature article, we discuss the current state-of-the-art in the field of bipolar electrochemiluminescence (BE–ECL), focusing mainly on the advances achieved during the last 5 years. At first, the fundamental concepts of BE and its synergy with ECL are presented, followed by a description of the most recent applications. Afterwards, emerging trends of bipolar ECL are discussed.

Fundamentals of bipolar electrochemiluminescence

From a thermodynamic point of view, BE can be easily classified into two categories, namely endogenous or exogenous bipolar electrochemistry (enBE or exBE, respectively), according to the driving force that induces the polarization. It is achieved either by coupling thermodynamically spontaneous redox reactions ($\Delta_r G < 0$, enBE) or by applying an external electric field (ε) ($\Delta_r G > 0$, exBE). However, an additional ingredient is required to properly consider a system as being bipolar, which is an asymmetry of the reactivity in space (*i.e.*, site-selective electrochemical processes). In other words, well-defined anodic and cathodic spatial regions, located at opposite extremities of the object, are necessary. Although the principles of enBE and exBE have been extensively explored, the majority of the bipolar ECL platforms are based on exogenous systems. Thus, in this section, the theoretical aspects of exBE coupled with ECL and different applications of this approach are briefly summarized.

BPE–ECL configuration

For exogenous bipolar systems, the experimental configuration is composed of a high-voltage power supply connected to two feeder electrodes to apply the electric field, and a conducting object positioned between these feeder electrodes without direct contact.[28,29] The endogenous bipolar electrode system operates through coupled spontaneous redox reactions enabled by hybrid electrodes composed of dissimilar metals (*e.g.*, Pt–Mg or Mg–Fe),[40] where the inherent potential difference between the metals drives the electron flow without using any external power input. In this configuration, the anodic metal undergoes oxidation, while the cathodic metal triggers reduction, creating a self-sustaining electron flux through the device. Practically, it resembles a short-circuited battery, with thermodynamically spontaneous reactions that are determined by the standard redox potentials of the constitutive metals.

The performance of bipolar electrodes is largely determined by the choice of electrode materials, which directly affects the electron transfer and the resulting luminescence efficiency.[41] Currently used electrode materials can be categorized into three main types: noble metals (*e.g.*, Au, Pt, and their nanoparticles) exhibit excellent conductivity and catalytic activity, but are prone to surface oxidation in aqueous media;[42–44] carbon-based materials (including various nanocarbons) are widely adopted due to their good conductivity and low cost, with inkjet printing and other screen printing techniques enabling the production of multifunctional electrode arrays;[45] transparent metal oxides (such as indium tin oxide, ITO) are ideal for ECL imaging thanks to their optical transparency, and their intrinsic conductivity can be further enhanced by doping strategies. Notably, novel electrode materials continue to emerge. For instance, Z. Wang in collaboration with our team demonstrated that stainless steel BPE can simultaneously promote both anodic and cathodic ECL of luminol.[46] Additionally, silicon semiconductor-based BPEs have enabled photo-induced ECL, upconverting infrared light into visible emission.[37]

Furthermore, due to its wireless nature, BE allows addressing a large number of conducting objects simultaneously, facilitating multiple analyte quantifications. For this, photolithography is commonly used for preparing BPEs, enabling the fabrication of highly accurate, complex and customizable electrode arrays. However, the stepwise preparation process is tedious and time-consuming, and cannot afford nanoscale electrode arrays. Recently, laser-assisted fabrication was explored as an alternative to photolithography. With this method, laser-induced graphene (LIG) or graphene oxide electrodes were designed.[47–51] By means of a miniaturized 3D-printed platform, a smartphone was employed to both power a LIG-based BE–ECL system and capture the ECL emission.[48,49] This setup was successfully used for the simultaneous quantification of vitamin B12 and vitamin C, demonstrating the impact of BE–ECL in multiplexed applications.[48]

Exogenous bipolar electrochemiluminescence

Commonly, an exBE-based ECL platform consists of a BPE positioned between two feeder electrodes, immersed in an electrolytic solution, containing the appropriate luminophore/co-reactant system. Under these conditions, the magnitude of ΔV across the BPE can be estimated using eqn (1), where l is the length of the BE.

$$\Delta V = \varepsilon \times l \quad (1)$$

As stated previously, redox reactions occur at both extremities of the BPE only when ΔV overcomes the ΔV_{min} associated with a set of involved electroactive species, which, in the case of ECL systems, consist of the luminophore/co-reactant and a sacrificial redox probe.[52] For example, in the presence of an aqueous solution of $[Ru(bpy)_3]^{2+}$/TPrA, the reactions occurring at the anodic (δ^+) and cathodic (δ^-) poles of the BPE are described using eqn (2)–(4):

Anode:

$$[Ru(bpy)_3]^{2+} \rightarrow [Ru(bpy)_3]^{3+} + e^- \quad (2)$$

$$TPrA \rightarrow TPrA^{\bullet+} + e^- \quad (3)$$

Cathode:

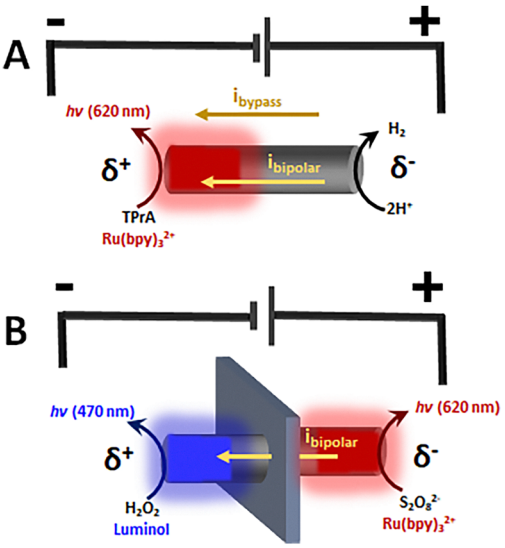

Fig. 1 Illustration of the (A) open and (B) closed BE experimental configurations, with a representation of the corresponding redox reactions involving the $[Ru(bpy)_3]^{2+}$/TPrA, $[Ru(bpy)_3]^{2+}/S_2O_8^{2-}$ and luminol/H_2O_2 systems, the anodically and cathodically polarized extremities (δ^+ and δ^-, respectively), the current flow and distribution and the colour of the resulting ECL emission zones.

$$2H^+ + 2e^- \rightarrow H_2 \quad (4)$$

Following these electrochemical reactions, the electrogenerated radical cation $TPrA^{\bullet+}$ loses a H^+ to form the neutral $TPrA^{\bullet}$ radical. The latter is a strong reducer that reacts with the oxidized form of the luminophore producing $[Ru(bpy)_3]^{2+\star}$, which emits light at the anodic pole of the BPE (Fig. 1A). It is important to highlight that in this so-called open configuration rather high voltages are required between the feeder electrodes to trigger the coupled reactions since the bipolar current ($i_{bipolar}$), passing through the BPE, is often limited by the bypass current (i_{bypass}) induced across the electrolytic solution. This effect can be minimized by employing a high resistance electrolyte or by using a closed BE configuration, in which the applied potential is forced to drop between the extremities of the BPE, thus decreasing the required voltage (Fig. 1B). In addition, such a configuration allows physical separation of the anodic and cathodic solutions, avoiding contamination from products formed at the opposite feeder electrodes.[26,53] Moreover, this closed set-up facilitates the simultaneous use of different luminophore/co-reactant systems or different solvents (aqueous and organic) in each electrolytic compartment.

Control and mapping of BPE polarization

From a fundamental point of view, in BE the length of the anodic and cathodic regions extends with stronger electric fields. As a consequence, the fraction of the BPE, having the proper potential to trigger the ECL reactions, is electric field-dependent.[54] Hence, ECL has been used as an optical readout of the potential gradient established across the BPE.[38,39,55,56] For example, the ECL emission produced by luminol/H_2O_2 at the anodic pole of a conducting polymer (poly-3,4-ethylenedioxythiophene, PEDOT) was used to map the electric properties along the material (Fig. 2A).[57] This approach has been extended to the efficient imaging of the potential gradient distribution produced in bipolar electrochemical cells with different configurations and to investigate the cathodic reactivity of luminol.[58–61] From the classic open configuration to cylinder-based setups, well-defined anodic ECL patterns were obtained, which are in agreement with the theoretical distribution of solution potential around a BE (Fig. 2B).[62] The magnitude of the interfacial potential difference is a key component of the potential composition of BE, and it significantly affects the effective control of redox reactions. In another study, a novel approach was established to modulate and control redox reactions at the BPE using an ion-selective membrane (ISM).[63] By forming a polymeric Na ISM on part of the BPE, the potential differences at the cathodic and anodic poles can be independently regulated. This study demonstrated significant changes in ECL intensity in both open and closed bipolar systems by varying the ISM location and primary ion concentrations. Folded BPE structures with an ISM either at one or both ends further enhance potential control. This technique offers improved controllability over redox reactions, making it a promising advancement for BE devices.

More recently, the polarization gradient was optically monitored through the annihilation ECL mechanism.[64] In this case, the oxidized and reduced forms of $[Ru(bpy)_3]^{2+}$, produced at the anode and cathode of the BE, respectively, react in order to populate the excited state of the luminophore. The synergy between the asymmetric reactivity and an electro-migrating mechanism generates an electric field-dependent anodic ECL

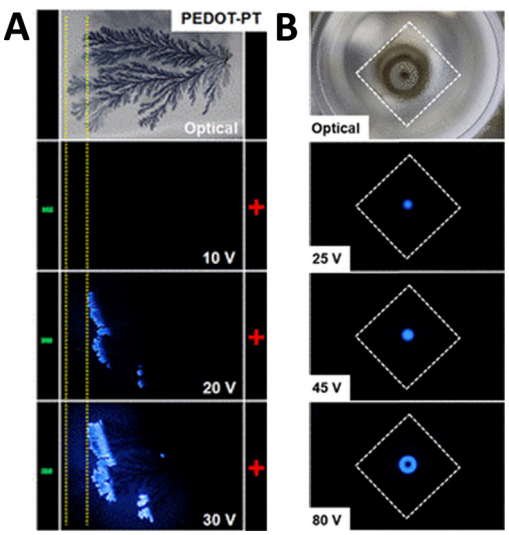

Fig. 2 (A) Photographs of the luminol/H_2O_2 ECL emission produced on a PEDOT–Pt hybrid BPE as a function of the applied potential (indicated in the figure). The dashed lines represent the position of Pt along the BE. Reproduced from ref. 57 with permission from American Chemical Society, copyright 2023. (B) Photographs of the ECL emission of luminol/H_2O_2 produced on an ITO plate by using a bipolar cell with a cylindrical configuration at different applied potentials (indicated in the figure). The dashed line represents the position of the BE. Reproduced from ref. 62 with permission from American Chemical Society, copyright 2021.

emission. Furthermore, there was an increase of the ECL intensity when using a double BPE system due to the electromigration of the ionic species formed at each extremity of two BPEs facing each other.

In addition, the electroactivity of silicon-based BPEs was studied as a function of the applied electric field. For this, the ECL emission of the $[Ru(bpy)_3]^{2+}$/TPrA system allows visualization of the influence of the bipolar current on the reactivity of the silicon-based BPEs. As the external electric field increases, the oxidized region of silicon expands, passivating the surface, which is reflected by a gradual depletion of the ECL emission zone.[65,66] Nevertheless, in all the above-mentioned examples, the potential distribution of only one pole of the BPE was achieved. Recently, Zhou *et al.* reported the mapping of the complete potential distribution across a BPE.[67] For this, the high reactivity of Mg was used to trigger the spontaneous reductive-oxidation mechanism of the $[Ru(bpy)_3]^{2+}/S_2O_8^{2-}$ system, producing a homogenous ECL emission on the entire surface of the BPE. When applying a high enough external electric field, there was a site-selective decrease and increase in the ECL intensity at the anode and cathode of the Mg–BPE, respectively. In addition, by fine-tuning the spatial distribution of the global electric field, more sophisticated ECL patterns were readily produced.

Signal amplification strategies in BE–ECL

As it is well-established, the performance of BE-based ECL processes is intimately related to the electrochemical stability of the luminophore, the thermodynamic difference between the two electrogenerated products and the nature and spatial arrangement of the BPEs. For example, Liu *et al.* developed an ultrasensitive BE–ECL immunoassay for the quantification of myoglobin.[68] In this case, the *in situ* reduction of $HAuCl_4$ to Au nanoparticles does enhance the conductivity of the sensing pole while amplifying the ECL signal generated at the anode. Alternatively, an MXene was used as the BPE substrate, due to its high electroactive surface area and electrical conductivity.[69] In this setup, the anodic ECL emission was further enhanced by the presence of immobilized triangular Ag nanoparticles *via* surface plasmon resonance. Moreover, the use of uniformly structured interdigitated BPE arrays with a different gap between the cathodic and anodic terminals has been proposed.[44] This involves the redox cycling of the $[Fe(CN)_6]^{3-}/[Fe(CN)_6]^{4-}$ redox pair, occurring between two closely spaced electrodes. While the redox cycling takes place in the sensing channel of the BPE, ECL emission is produced at the reporting chamber. A direct correlation between the gap size and the intensity of the ECL emission was demonstrated. The quantification of cell surface markers was achieved by coupling the interdigitated BPE arrays to a microfluidic device.[70,71] However, interference between the responses of each BPE was found to limit this approach. With a similar approach, a matrix of interwoven spiral BPEs with a 0.5 μm gap was used, improving the sensitivity tenfold, in comparison with the interdigitated BPE array system.[72] Alternatively, by adjusting the ratio between the cathodic and anodic areas, a concentrated ECL emission was produced, thus enhancing the sensitivity.[73] More recently, Yee *et al.* proposed a sandwich architecture in which an ECL active layer is positioned between two coplanar electrodes.[74] A floating BPE modulates the electric field distribution within the active layer, enabling the use of opaque and electrochemically stable noble metals as driving electrode materials, while allowing light emission to operate through the transparent floating electrode. The floating-electrode system presents an extended lifespan (above 1 hour), in comparison with conventional sandwich-type ECL devices.

The extensive progress in the understanding of the fundamentals involved in BE–ECL enables different alternatives to improve the efficiency, sensitivity, and versatility of this approach. As mentioned previously, this has led to remarkable advancements in multimodal detection strategies, multiplexed quantification and bipolar ECL microscopy.

Applications of bipolar electrochemiluminescence

Ratiometric sensing

In clinical and environmental applications, the relative ratio between two different signals is often used to provide a more precise and reliable measurement, minimizing the impact of possible instrumental interferences. Such an approach enhances the precision and robustness of the sensors by leveraging the BE–ECL synergy.[75,76] As stated above, the spatial separation of the anodic and cathodic poles in the closed BE systems allows simultaneous monitoring of two redox reactions, enabling the generation of multiple signals for ratiometric analysis. For example, Wang *et al.* developed an ECL biosensor for miRNA-141 detection using a system with two reservoirs connected by a constant resistor.[77] Boron nitride quantum dots at the cathode coupled with the $[Ru(bpy)_3]^{2+}$/TPrA system at the anode served as the dual ECL source. However, the main challenge in ratiometric strategies based on bipolar ECL arises from the unbalanced quantum efficiency of both anodic and cathodic luminophores, leading to inaccurate ratio-based detection. Thus, the molecular tailoring of novel luminophores and co-reactants that generate stable emissions with comparable strength is highly desired.

Multicolor and multiplex detection

Alternatively, wireless multicolour ECL systems have gained significant attention due to the synergistic effect between potential-resolved and spectral-resolved signals, which enables the simultaneous detection of multiple signals.[78–82] The most common multicolour BE–ECL systems use mixtures of Ru(II) and Ir(III) complexes.[79–85] For example, $[Ir(ppy)_2(pic\text{-}OMe)]$, $[Ir(ppy)_2(acac)]$, and $[Ru(bpy)_3]^{2+}$ (with pic = picolinate, ppy = 2-phenylpyridine and acac = acetylacetonate ligands) serve as blue, green, and red ECL luminophores, respectively.[79] By changing the applied voltage, these luminophores produce a combined emission that covers the entire visible spectrum. Moreover, the colour of the ECL emission at the anodic extremity can be easily fine-tuned by reactions occurring at the cathode due to changes in interfacial potentials and faradaic currents. With such a platform, the optical detection of

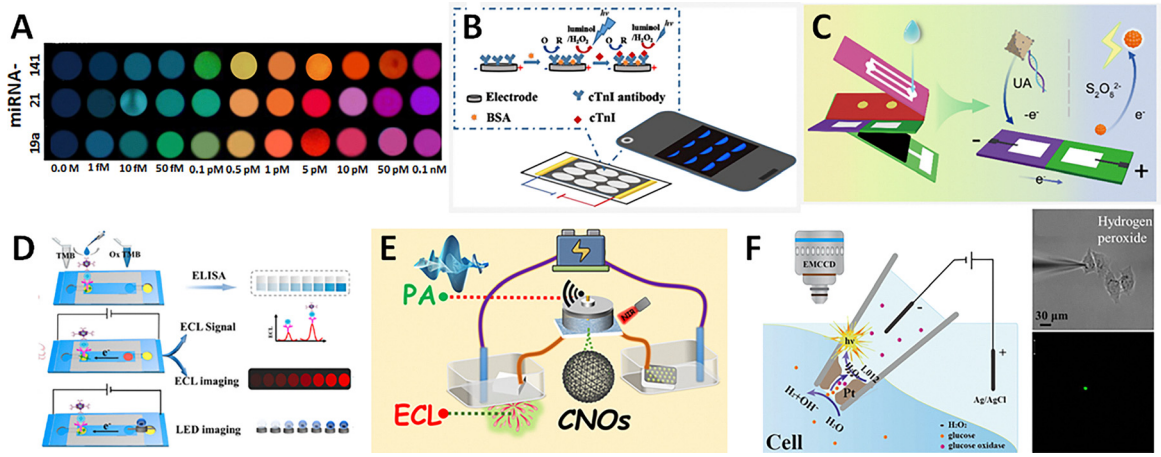

Fig. 3 (A) Colour change response as a function of the concentration of miRNA (indicated in the figure) obtained from the bipolar ECL emission of a mixture of three different luminophores [Ir(ppy)$_2$(pic-OMe)], [Ir(ppy)$_2$(acac)] and [Ru(bpy)$_3$]$^{2+}$ in a 1 : 0.2 : 0.1 ratio. Reproduced from ref. 79 with permission from American Chemical Society, copyright 2024. (B) Assembly strategy of the label-free ECL immunosensor for cTnI based on the carbon ink SEES. Reproduced from ref. 88 with permission from American Chemical Society, copyright 2022. (C) Illustration of the self-cleaning operation of a paper-based BE–ECL device (left panel) and analytical mechanism for the quantification of M.SssI MTase (right panel). Reproduced from ref. 92 with permission from American Chemical Society, copyright 2022. (D) Representation of the closed BE set-up used during the quantification of CEA *via* ELISA (top), ECL (middle) and LED imaging (bottom). Reproduced from ref. 95 with permission from American Chemical Society, copyright 2024. (E) Schematic illustration of the wireless ECL–photoacoustic (PA) dual-signal output biosensor for the detection of ovarian cancer markers. Reproduced from ref. 96 with permission from American Chemical Society, copyright 2022. (F) Illustration of the BE–ECL detection at a porous platinum-coated nanopipette for intracellular wireless electroanalysis (left panel) and optical pictures of the bright-field (top) and ECL emission (bottom) of the nanopipette during the electroanalysis of intracellular hydrogen peroxide. Reproduced from ref. 98 with permission from Wiley-VCH, copyright 2020.

three miRNAs was achieved based on variations of colour, providing a rapid and effective method to diagnose prostate cancer (Fig. 3A). In addition, to enable the simultaneous detection of multiple targets, this approach paves the way for new possibilities in the development of multiplex detection systems.

A single-electrode electrochemical system (SEES)[23,86,87] for wireless multiplex ECL analysis of cardiac troponin I (cTnI), a specific biomarker of acute myocardial infarction, was developed (Fig. 3B).[88] The SEES was designed by attaching an insulating sticker with multiple holes to a single carbon ink screen-printed electrode. Compared to multi-electrode array systems, the SEES is characterized by its simplicity and cost-effectiveness. In addition to these approaches, paper-based microfluidic BE–ECL detection chips can be fabricated using inkjet, wax, or screen printing.[89–92] Using these methods enables the fabrication of patterns, and rational partitions were obtained, allowing the simultaneous detection of two or more components on a single platform. For example, Zhang *et al.* introduced a hand-drawn paper-based BE–ECL platform for the quantification of M.SssI methyltransferase (M.SssI MTase) (Fig. 3C).[92] In this case, the quenching of the ECL emission produced by the MnS:CdS@ZnS/$S_2O_8^{2-}$ system, occurring at the cathode of the BPE, was used as the optical analytical signal. By employing pencil-drawn graphite circuits as wires and electrodes, the fabrication process was greatly simplified, and costs were significantly reduced. Furthermore, the integration of a multilayer origami structure improved fluid handling, minimized background interference and enhanced self-cleaning efficiency.

Multimodal readout

To improve accuracy and minimize false positives, bipolar ECL can be easily coupled with alternative physicochemical readouts, produced by colorimetric, photoacoustic, and electrochromic methods.[93–97] Liu *et al.* recently developed a triple-reading immunosensor, combining the classic enzyme-linked immunoassay (ELISA) and the optical readout produced by two different light sources, ECL and light emitting diodes (LEDs) (Fig. 3D).[95] The ELISA detection of cancer embryonic antigen (CEA) was incorporated into the BE sensing platform at the cathode *via* an immunoreaction, while [Ru(bpy)$_3$]$^{2+}$ was introduced at the anode for ECL measurement. Additionally, LED imaging, powered by the electron flux produced by the sensing reaction, produces an additional readout for the quantification of CEA. Alternatively, an ECL–photoacoustic dual-signal output biosensor for the detection of ovarian cancer markers was developed (Fig. 3E).[96] For this, while the sensing ECL emission is produced at the anode and the hydrogen evolution reaction occurs at the cathode, carbon-based nano-onions produce the photoacoustic readout *via* a thermal expansion mechanism. Although, compared to classic ECL measurements, BE–ECL offers notable advantages in multi-output sensing, such as improved spatial readout separation and easy independent signal acquisition, several challenges associated to signal stability, precise control of the electron transfer and signal interferences remain.

Micro- and nano-imaging

Recently, ECL analysis at both the micro- and nanoscale has revolutionized the study of dynamic processes down to the

cellular and molecular levels.[98–109] In this context, bipolar electrochemical microscopy is a powerful tool for wireless single-cell electrochemical analysis. For example, a porous platinum-coated nanopipette, acting as an open bipolar ECL device, was designed for intracellular wireless analysis (Fig. 3F).[98] The porous platinum coating acts as a BPE enabling cytosol extraction and ECL generation by the L-012/H_2O_2 system, with L-012 being a luminol analogue that is soluble at neutral pH. With such a device, electroanalysis of intracellular hydrogen peroxide, glucose, and sphingomyelinase activity *in vivo* was achieved by applying a low driving voltage, minimizing cell disruption. Following a similar approach, wireless electrochemical visualization of intracellular proteins in single cells using BE–ECL was achieved.[99] Submicron-sized single-walled carbon nanotubes functionalized with antibodies conjugated with an ECL luminophore were used to target antigens in the nucleus of MCF-7 cells. A low applied voltage enables the ECL emission from L-012 due to the efficient voltage drop caused by the confined anodic and cathodic compartments. Alternatively, advanced microfabrication techniques facilitate the design of multi-electrode arrays for high-resolution ECL imaging.[100–105,110] For example, arrays of multi-electrode fibres were designed by filling porous plates with carbon paste or by thermal drawing,[101,103] and micro-Au electrodes were obtained by electroless plating on track-etched membranes.[102] These devices have been used for bipolar ECL microscopy, enhancing the spatial resolution. Additionally, by optimizing BE designs and employing confinement effects, the developed systems require lower driving voltages, improving energy efficiency.

Emerging trends

Despite the outstanding developments involving exBE-based ECL approaches, novel and more sophisticated wireless light-emitting systems are continuously designed. This is mainly motivated by the inherent advantages of BE. For example, due to its wireless nature, it is possible to design ECL-based dynamic systems, enabling the direct tracking of motion at high spatial and temporal resolution. Moreover, by exploiting the versatility of BE, it is possible to combine multiple light sources, operating in different emission modes, thus paving the way for the development of easy and straightforward multimodal light-emitting platforms. Hence, in this section, we summarize different emerging trends in the field of BE–ECL.

Spatially-constrained and interfacial systems

Building upon the previously discussed concepts of ECL and BE systems, an interesting area of study lies in the development of spatially-constrained and interfacial systems. These are particularly relevant for addressing challenges related to the polarization of small conductive objects, which, according to eqn (1), typically require large electric fields.[111] For example, a microfluidic device composed of a rhombus-shaped Au microelectrode integrated into a solid-state micropore was designed. Under these conditions, the Au microelectrode is polarized remotely by applying a mild voltage (10 V). The micropore focuses the electric field within a small region, boosting the local potential gradient, while also eliminating unnecessary energy dissipation in the surrounding solution. This design allows the threshold polarization potential to be decreased by 100-fold. In a similar way, Wang *et al.* demonstrated that BE in microchannels decreases the required voltage, thereby improving the ECL emission.[112] This setup was used to develop a biosensing system that integrates photonic crystal structural colour coding with BE–ECL imaging for multiplex quantification. In this work, by increasing the cell length/microchannel width ratio, a decrease of the driving voltage to trigger the electrochemical reaction is observed. Alternatively, the ECL emission within a 2D nanoconfined environment composed by a surfactant-based bubble was reported.[113] For this, soap bubbles loaded with 2D graphene microparticles, acting as BPEs, and the $[Ru(bpy)_3]^{2+}$/2-(dibutylamino)ethanol (DBAE) system produce ECL emission when applying a low external electric field (Fig. 4A). This decrease, by up to three orders of magnitude in comparison with conventional systems, is associated with the spatial confinement within the ultrathin soap bubble layer. This 2D environment enhances the collision frequency between target molecules and BPEs, while simultaneously minimizing the bypass currents.

Furthermore, surface-confined ECL was achieved by taking advantage of the interface formed between a water/oil (w/o) mixture. For this, amphiphilic Janus microbeads, acting as BPEs, were placed at the w/o interface.[114] Due to the difference in the polarity of the two immiscible liquids, the phase separation resembles a ''pseudo-closed'' bipolar cell (Fig. 4B). By applying a high enough electric field and in the presence of a hydrophilic and a hydrophobic luminophore/coreactant system, at the aqueous and organic phases, respectively, two well-defined ECL emissions were produced. This indicates that, despite the presence of potential gradients along the particle, mass transport across the liquid/liquid interface remains partially active, facilitating the electrochemical reactions. Moreover, by fine-tuning the orientation of the electric field, blue and red hemispherical or quarter-sphere-shaped ECL emission regions were produced (Fig. 4B).

Dynamic ECL systems

As stated above, the design of mobile devices capable of producing ''on-board'' light has become a powerful tool for the study of complex dynamics and interactions at the macro-, micro- and nanoscale.[115–119] When a BPE is rotated within a static DC electric field, alternating bipolar currents are induced, which can be extracted from feeder currents (i_{feeder}) using a lock-*n* amplifier (Fig. 5A).[116] ECL is used to visualize the potential drop at the interface of the rotating BPE. With this configuration, the ECL intensity not only displays spatial heterogeneity across the BPE surface, but also undergoes dynamic angular modulation, with the emission maximum being correlated to the BPE's alignment with respect to the applied field. This orientation-dependent behaviour arises from asymmetric charge transfer kinetics, dictated by the electrode's rotational position. The ECL peak occurs shortly after the BPE passes the orthogonal direction, as several

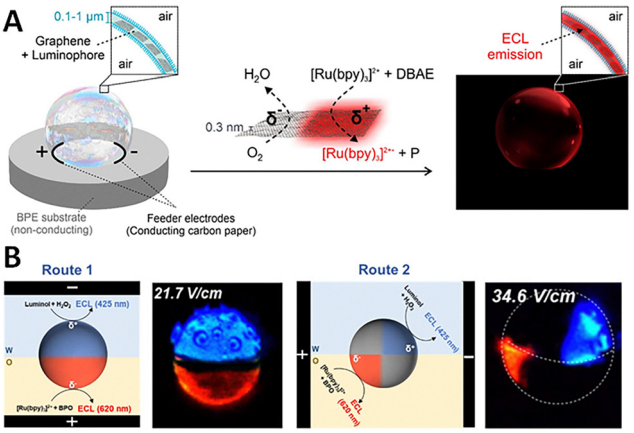

Fig. 4 (A) Illustration a thin layer soap bubble acting as a 2D nanoconfined environment containing graphene sheets and the $[Ru(bpy)_3]^{2+}$/DBAE ECL system, with a representation of the redox reactions and the ECL emission. Reproduced from ref. 113 with permission from the Royal Society of Chemistry, copyright 2022. (B) Representation and optical images of the wireless ECL emission from amphiphilic Janus particles at the W/O interface obtained with two different electric field orientations: perpendicular (left panel) and parallel (right panel) to the W/O interface. Reproduced from ref. 114 with permission from the Royal Society of Chemistry, copyright 2024.

reaction steps are required prior to the formation of the excited-state 3-aminophthalate luminophore. Additionally, from a theoretical point of view, when using a rotating BPE, it is possible to map the angular dependence of the induced polarization potential. For example, it was demonstrated that an alternating ECL emission is generated during the rotation of Fe–Au coated BPEs. The oscillating light emission is intimately related to the alignment of the BPE with respect to the electric field. Based on this principle, a BE–ECL rotor was designed for the dynamic quantification of glucose.[117] In this case, the motion of an iron wire, acting as the BPE, is guided by a rotating-magnetic field. In the presence of H_2O_2, produced by the enzymatic oxidation of glucose, and by applying a high enough electric field, ECL emission from L-012 is produced. Interestingly, glucose detection was achieved simultaneously at both the cathodic and anodic extremities of the BPE, following two different mechanisms. Moreover, rotating BE–ECL systems facilitate the direct visualization of the corresponding mass transport regime.

For example, the impact of controlled hydrodynamic conditions, associated to rotational displacement of the ECL emission, was recently studied. For this, the ECL emission of the $[Ru(bpy)_3]^{2+}$/TPrA system was produced at the anode of a rotating disk electrode, acting as the BPE (Fig. 5B).[118] Under these conditions, the ECL-emitting region moves gradually from the anodic extremity to the cathodic pole of the BPE as a function of the rotation speed. The hydrodynamic convection directly impacts the shape of the ECL emission, shifting from an "ECL croissant" to a ring-like pattern. It was demonstrated that the shape of such ECL patterns is directly controlled by the rotation speed, chemical reactivity and the wirelessly induced polarization.

Self-powered systems

Finally, self-driven optical readouts have emerged as interesting alternatives to replace externally-triggered imaging approaches. Although there are few examples, they take advantage of thermodynamically- and kinetically-favoured redox reactions occurring in well-defined spatial regions within a single object.[8,120] For example, the electrocatalytic activity towards the oxygen reduction reaction of different Pt-based catalysts was evaluated by changes in fluorescence occurring at the anode of a BE array.[121] The use of ECL as optical readout allows avoiding the necessity of additional light sources, in comparison with fluorescence-based approaches. However, a thermodynamically-favoured source of electrons is

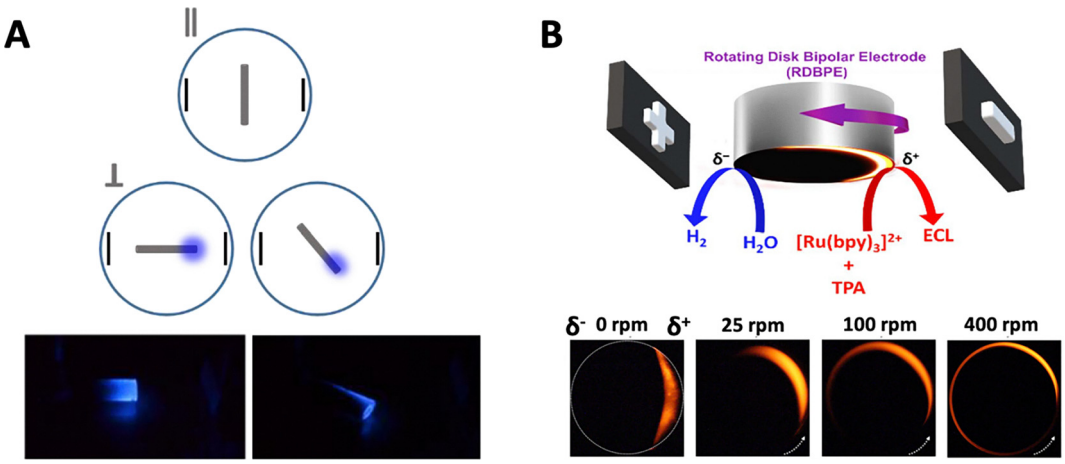

Fig. 5 (A) Illustration of the dependency of i_{feeder} and ECL intensity on the orientation of the BPE. Maximum i_{feeder} occurs when the BPE is orthogonally aligned to the feeder electrodes and minimum occurs under parallel alignment (top scheme); images of luminol ECL at the anodic pole in different orientations at V_{app} = 4 V (bottom). Reproduced from ref. 116 with permission from Elsevier, copyright 2017. (B) Schematic diagram of a rotating disk bipolar electrode with a representation of the redox reactions and the produced shape of the ECL emission (top scheme) and optical pictures of the $[Ru(bpy)_3]^{2+}$/TPrA ECL emission as a function of the rotational speed at a constant electric field of 8.3 V cm^{-1}. The dotted circle and arrow indicate the position and direction of the rotation, respectively. Reproduced from ref. 118 with permission from the Royal Society of Chemistry, copyright 2024.

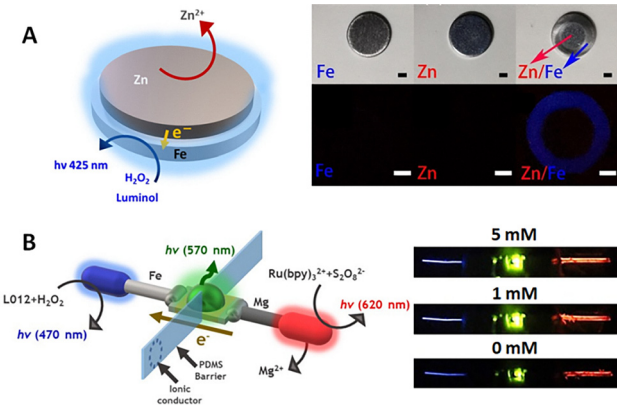

Fig. 6 (A) Illustration of the Zn/Fe self-powered ECL device with a representation of the corresponding reactions (left panel) and photographs of metallic disks with different compositions (indicated in the figure) in the absence (top) and presence (bottom) of a luminol/H_2O_2 solution (right panel). Reproduced from ref. 8 with permission from Wiley-VCH, copyright 2024. (B) Scheme of the endogenous hybrid light-emitting array with a representation of the associated redox reactions, the electron flux and the colour of the resulting light emission (left panel), and optical pictures of the ECL/LED emissions generated by the multimodal array in the presence of the $[Ru(bpy)_3]^{2+}/S_2O_8^{2-}$ and L-012/H_2O_2 ECL systems at the anodic and cathodic compartments, respectively, and increasing $S_2O_8^{2-}$ concentrations (right panel). Reproduced from ref. 122 with permission from the Royal Society of Chemistry, copyright 2023.

required to power the ECL emission. Due to their relatively high thermodynamic redox potential, Zn and Mg (−0.76 V and −2.36 V *vs.* NHE) can act as efficient on-board power sources. For example, Liu *et al.* designed a bimetallic Zn/Fe self-powered ECL device by coupling the oxidation of Zn and the reduction of H_2O_2 at Fe surface.[8] Under these conditions, the reactive oxygen species generated during the reduction of H_2O_2 react with luminol to trigger the ECL emission (Fig. 6A). With this enBE system, the quantification of ascorbic acid (a radical quencher) was achieved with a good detection limit (0.31 μM). Furthermore, the concept of enBE has become an interesting alternative to design self-powered multimodal optical platforms based on two different light sources. For instance, a multicolour light-emitting device was designed by coupling the fundamentals of enBE, ECL and LEDs.[120] The endogenous bipolar electrode array was composed of three modified LEDs with different colours (*i.e.* yellow, green and blue). In each diode, the driving force that powers the light emission is the flux of electrons produced by the oxidation and reduction of Mg and H^+ taking place at the anode and cathode of the LED, respectively. In addition, ECL was introduced at the anode by taking advantage of the spontaneous reductive-oxidation mechanism of the $[Ru(bpy)_3]^{2+}/S_2O_8^{2-}$ system powered by Mg. With such a device, light emission with four different wavelengths was produced, which, according to the Nernst equation, can be easily fine-tuned by the physicochemical properties of the solution. Following the same principle, a single self-driven multimodal light-emitting bipolar electrode was designed.[122] In this case, a physical barrier produces an anodic and a cathodic compartment, containing the $[Ru(bpy)_3]^{2+}/S_2O_8^{2-}$ and L-012/H_2O_2 ECL systems, respectively (Fig. 6B). While in the anodic compartment, once again, the spontaneous oxidation of Mg triggers the reductive-oxidation mechanism of $[Ru(bpy)_3]^{2+}/S_2O_8^{2-}$, the generated flux of electrons from the anode to the cathode of the device powers the green emission of the LED. Simultaneously, a fraction of the electrons is consumed in the cathodic compartment inducing the characteristic blue emission of the L-012/H_2O_2 ECL system.

Conclusions

The integration of ECL and BE has driven the development of new methodologies and devices with innovative applications in bioanalysis, multiparametric detection, and electrochemical microscopy. Recent studies have not only improved the sensitivity and efficiency of these systems, but have also opened opportunities to explore new fundamental concepts and their implementation in advanced applications. In the future, one of the main challenges and areas of opportunity lies in the refinement of autonomous and self-powered systems, in which the combination of spontaneous redox reactions and the concomitant activation of optoelectronic devices, such as LEDs, will enable the development of completely independent sensors. Likewise, the design of platforms with spatial confinement and optimized electrochemical interfaces represents a promising strategy to reduce activation voltages and enhance selectivity in analyte detection. The study of dynamic systems, where electrochemistry and hydrodynamics interact in real-time, is another emerging field with great potential. The manipulation of ECL emission patterns through flow and motion control opens possibilities for real-time visualization of electrochemical processes and the optimization of rotational sensors for high-resolution biochemical analysis. Finally, employing BE–ECL with multimodal and multiplexed detection strategies will expand their applications in clinical diagnostics, environmental monitoring, and the development of low-cost portable devices. The synergy between these approaches offers a promising pathway for advancing both fundamental research as well as the development of innovative analytical technologies. This integration enables the creation of compact, stable, and user-friendly detection platforms, with increasing potential for incorporation into portable devices, such as the use of smartphones to acquire imaging capability. Moreover, the AI-assisted processing of images could be an interesting approach. These developments aim to enhance both the accessibility and performance of electrochemical sensing systems. In parallel, the design of new luminophores with balanced anodic and cathodic emissions, alongside a deeper understanding of electric field distribution and interfacial reaction dynamics on the BPE surface, will be essential for improving system efficiency and selectivity. Controlling redox processes under confined or dynamic conditions also remains crucial. For instance, in multiphase environments, it represents a valuable strategy for developing more sensitive and selective detection approaches. Furthermore, the emergence of self-powered and dynamic BPE–ECL systems is a versatile platform to investigate complex physicochemical phenomena and to engineer autonomous

analytical tools with a low energy requirement. Together, these advances will establish BPE–ECL as a promising technology in the future landscape of electrochemical sensing and biochemical analysis.

Conflicts of interest

There are no conflicts to declare.

Data availability

No primary research results, software or code have been included and no new data were generated or analysed as part of this review.

Acknowledgements

R. Z. acknowledges the China Scholarship Council (CSC), the National Natural Science Foundation of China (22264020) and the Natural Science Foundation of the Ningxia (2023AAC03328) for supporting her research. L. R. A.-A. acknowledges the University of Bordeaux for her PhD scholarship. G. S. is grateful for funding from the Agence National de la Recherche (ANR) *via* the project CHIRA-SENSEO (ANR-23-CE42-0004-01) and the authors thank the ANR (MAPICS, ANR-23-CE42-0018-04) and the CNRS (Sino-French International Research Network ELECTROSENS) for financial support.

References

1 S. Rebeccani, A. Zanut, C. I. Santo, G. Valenti and F. Paolucci, *Anal. Chem.*, 2022, **94**, 336–348.
2 M. Hesari and Z. Ding, *J. Electrochem. Soc.*, 2015, **163**, H3116–H3131.
3 Z. Liu, W. Qi and G. Xu, *Chem. Soc. Rev.*, 2015, **44**, 3117–3142.
4 N. Sojic, *Analytical Electrogenerated Chemiluminescence: From Fundamentals to Bioassays*, The Royal Society of Chemistry, 2019.
5 M. Chen, Z. Ning, K. Chen, Y. Zhang and Y. Shen, *J. Anal. Test.*, 2020, **4**, 57–75.
6 Y. Yan, L. Ding, J. Ding, P. Zhou and B. Su, *ChemBioChem*, 2024, **25**, e202400389.
7 Y. Wei, H. Qi and C. Zhang, *Chem. Commun.*, 2023, **59**, 3507–3522.
8 H. Liu, A. Hussain, Y. T. Zholudov, D. V. Snizhko, N. Sojic and G. Xu, *Angew. Chem., Int. Ed.*, 2024, **63**, e202411764.
9 V. Gupta, F. Falciani, B. R. Layman, M. L. Hill, S. Rapino and J. E. Dick, *Chem. Biomed. Imaging*, 2025, **3**, 310–321.
10 B. R. Layman and J. E. Dick, *J. Am. Chem. Soc.*, 2023, **146**, 707–713.
11 X. Gou, Z. Xing, C. Ma and J.-J. Zhu, *Chem. Biomed. Imaging*, 2023, **1**, 414–433.
12 M. Belotti, M. M. T. El-Tahawy, L. J. Yu, I. C. Russell, N. Darwish, M. L. Coote, M. Garavelli and S. Ciampi, *Angew. Chem., Int. Ed.*, 2022, **61**, e202209670.
13 Y. Wang, S. Zhou, Y. Zheng, Y. Wang, Y. Hou, K. Wu, C. Huang, S. Liu, Y. Shen, R. Chen and Y. Zhang, *J. Am. Chem. Soc.*, 2025, **147**, 19380–19390.
14 K. Wu, R. Chen, Z. Zhou, X. Chen, Y. Lv, J. Ma, Y. Shen, S. Liu and Y. Zhang, *Angew. Chem., Int. Ed.*, 2023, **62**, e202217078.
15 Y. Fang, H. Yang, Y. Hou, W. Li, Y. Shen, S. Liu and Y. Zhang, *Nat. Commun.*, 2024, **15**, 3597.
16 Q. Sun, Z. Ning, E. Yang, F. Yin, G. Wu, Y. Zhang and Y. Shen, *Angew. Chem., Int. Ed.*, 2023, **62**, e202312053.
17 R. Chen, X. Wang, K. Wu, S. Liu and Y. Zhang, *Anal. Chem.*, 2022, **94**, 17625–17633.
18 S. E. Fosdick, K. N. Knust, K. Scida and R. M. Crooks, *Angew. Chem., Int. Ed.*, 2013, **52**, 10438–10456.
19 N. Shida, Y. Zhou and S. Inagi, *Acc. Chem. Res.*, 2019, **52**, 2598–2608.
20 N. Karimian, P. Hashemi, A. Afkhami and H. Bagheri, *Curr Opin. Electrochem.*, 2019, **17**, 30–37.
21 Y. L. Wang, J. T. Cao and Y. M. Liu, *ChemistryOpen*, 2022, **11**, e202200163.
22 S. F. Douman, E. Brennan, E. I. Iwuoha and R. J. Förster, *Anal. Chem.*, 2017, **89**, 11614–11619.
23 Z. Dong, Y. Chen, S. Xia, A. M. A. Alboull, A. Hussain, Y. Tian and G. Xu, *Anal. Chem.*, 2024, **96**, 18927–18931.
24 D. Ibañez, A. Heras and A. Colina, *Anal. Chem.*, 2017, **89**, 3879–3883.
25 S. F. Douman, D. Collins, L. R. Cumba, S. Beirne, G. G. Wallace, Z. Yue, E. I. Iwuoha, F. Melinato, Y. Pellegrin and R. J. Förster, *Chem. Commun.*, 2021, **57**, 4642–4645.
26 J. López-Asanza, D. Andrade-Alarcón, A. Molina and E. Laborda, *Electrochim. Acta*, 2025, **512**, 145417.
27 K. L. Rahn and R. K. Anand, *Anal. Chem.*, 2021, **93**, 103–123.
28 L. Bouffier, D. Zigah, N. Sojic and A. Kuhn, *Annu. Rev. Anal. Chem.*, 2021, **14**, 65–86.
29 L. Bouffier, D. Zigah, N. Sojic and A. Kuhn, *Encycl. Electrochem.*, 2021, 1–53.
30 G. Salinas, L. Bouffier, N. Sojic and A. Kuhn, *J. Solid State Electrochem.*, 2023, **28**, 1225–1231.
31 P. Chassagne, P. Garrigue and A. Kuhn, *Adv. Mater.*, 2024, **36**, e2307539.
32 G. Salinas and A. Kuhn, *Curr. Opin. Electrochem.*, 2025, **49**, 101612.
33 S. Grecchi, B. Bonczak, F. Malacarne, G. Salinas, R. Cirilli and S. Arnaboldi, *Chem. Commun.*, 2024, **60**, 10120–10123.
34 H. Chen, J. L. Anderson and R. K. Anand, *ACS Appl. Mater. Interfaces*, 2022, **14**, 18087–18096.
35 Y. Kokubo and H. Asoh, *ACS Omega*, 2023, **8**, 27024–27029.
36 Z. Qi, S. You and N. Ren, *Electrochim. Acta*, 2017, **229**, 96–101.
37 Y. Zhao, J. Descamps, B. Le Corre, Y. Leger, A. Kuhn, N. Sojic and G. Loget, *J. Phys. Chem. Lett.*, 2022, **13**, 5538–5544.
38 A. Arora, J. C. T. Eijkel, W. E. Morf and A. Manz, *Anal. Chem.*, 2001, **73**, 3282–3288.
39 K.-F. Chow, F. Mavré and R. M. Crooks, *J. Am. Chem. Soc.*, 2008, **130**, 7544–7545.
40 G. Salinas, A. L. Dauphin, C. Colin, E. Villani, S. Arbault, L. Bouffier and A. Kuhn, *Angew. Chem., Int. Ed.*, 2020, **59**, 7508–7513.
41 G. Valenti, A. Fiorani, H. Li, N. Sojic and F. Paolucci, *ChemElectroChem*, 2016, **12**, 1990–1997.
42 X. Li, X. Qin, Z. Tian, K. Wang, X. Xia, Y. Wu and S. Liu, *Anal. Chem.*, 2022, **94**, 7350–7357.
43 J. Wooa, J. Kim and J. Kim, *J. Electroanal. Chem.*, 2022, **906**, 115998.
44 J. S. Borchers, C. R. Campbell, S. B. Van Scoy, M. J. Clark and R. K. Anand, *ChemElectroChem*, 2021, **8**, 3482–3491.
45 F. Wang, Y. Qi, L. Ji, F. Qiao, Y. Chen, X. Xiong and Y. Liu, *Food Chem.*, 2024, **461**, 140842.
46 M. Feng, A. L. Dauphin, L. Bouffier, F. Zhang, Z. Wang and N. Sojic, *Anal. Chem.*, 2021, **93**, 16425–16431.
47 M. Bhaiyya, P. K. Pattnaik and S. Goel, *Microfluid. Nanofluidics.*, 2021, **25**, 41–48.
48 M. Bhaiyya, P. K. Pattnaik and S. Goel, *Sens. Actuators, A*, 2021, **331**, 112831.
49 M. Bhaiyya, P. Rewatkar, M. Salve, P. K. Pattnaik and S. Goel, *IEEE Trans. Nanobiosci.*, 2021, **20**, 79–85.
50 M. Salve, A. Mandal, K. Amreen, B. V. V. S. N. P. Rao, P. K. Pattnaik and S. Goel, *IEEE Trans. Instrum. Meas.*, 2021, **70**, 1–10.
51 M. Bhaiyya, P. K. Pattnaik and S. Goel, *Microchim. Acta*, 2022, **189**, 79–87.
52 J. López-Asanza, A. Molina and E. Laborda, *Electrochim. Acta*, 2025, **529**, 146345.
53 E. Laborda and A. Molina, *Curr. Opin. Electrochem.*, 2023, **39**, 101287.
54 E. Villani and S. Inagi, *Anal. Chem.*, 2025, **97**, 5837–5846.
55 F. Mavré, R. K. Anand, D. R. Laws, K.-F. Chow, B.-Y. Chang, J. A. Crooks and R. M. Crooks, *Anal. Chem.*, 2010, **82**, 8766–8774.
56 L. Gao, Y. Huang, S. Zhang, Y. Chen, S. Yan, H. Dai and B. Zeng, *Talanta*, 2024, **268**, 125301.
57 E. Villani, Y. Zhang, Z. Chen, Y. Zhou, M. Konishi, I. Tomita and S. Inagi, *ACS Appl. Polym. Mater.*, 2023, **5**, 6186–6198.

58 M. Wagner, Á. Brady, O. F. Doyle and R. J. Förster, *ChemElectroChem*, 2025, **12**, e202400506.
59 Á. Brady and R. J. Förster, *Anal. Chem.*, 2024, **97**, 410–418.
60 Á. Brady, M. Wagner and R. J. Förster, *Chem. Commun.*, 2024, **60**, 13000–13003.
61 M. Feng, A. L. Dauphin, L. Bouffier, F. Zhang, Z. Wang and N. Sojic, *Anal. Chem.*, 2021, **93**, 16425–16431.
62 E. Villani and S. Inagi, *Anal. Chem.*, 2021, **93**, 8152–8160.
63 N. A. A. Mutalib, A.-J. Hsueh, Y. Deng, M. Suzuki, C.-C. Wu, Y. Shirato and H. Suzuki, *J. Electrochem. Soc.*, 2024, **171**, 027502.
64 L. R. Arias-Aranda, G. Salinas, H. Li, C. F. Hogan, A. Kuhn, L. Bouffier and N. Sojic, *ChemElectroChem*, 2024, **11**, e202400522.
65 A. Ismail, S. Voci, L. Descamps, A. Buhot, N. Sojic, L. Leroy and A. Bouchet-Spinelli, *Chem. Phys. Chem.*, 2021, **22**, 1094–1100.
66 A. Ismail, S. Voci, P. Pham, L. Leroy, A. Maziz, L. Descamps, A. Kuhn, P. Mailley, T. Livache, A. Buhot, T. Leichlé, A. Bouchet-Spinelli and N. Sojic, *Anal. Chem.*, 2019, **91**, 8900–8907.
67 C. Zhou, L. R. Arias-Aranda, G. Salinas, L. Bouffier, Z. Wang, A. Kuhn and N. Sojic, *ChemElectroChem*, 2025, e202500012.
68 Y.-L. Wang, L.-Z. Zhao, C. Chen, S.-W. Ren, J.-T. Cao and Y.-M. Liu, *J. Electroanal. Chem.*, 2023, **930**, 117153.
69 S. M. R. Mortazavi, M. Hosseini, G. Xu, H. Naderi-Manesh and M. R. Ganjali, *Microchim. Acta*, 2024, **191**, 734–743.
70 Z. Dong, Y. Chen, S. Xia, A. M. A. Alboull, A. Hussain, Y. Tian and G. Xu, *Anal. Chem.*, 2024, **96**, 18927–18931.
71 J. S. Borchers, M. J. Clark, S. B. Van Scoy and R. K. Anand, *ChemElectroChem*, 2024, **11**, e202300345.
72 M. J. Clark, H. J. Moser and R. K. Anand, *ChemElectroChem*, 2024, **11**, e202400182.
73 A. J. Hsueh, N. A. A. Mutalib, Y. Shirato and H. Suzuki, *ACS Omega*, 2022, **7**, 20298–20305.
74 H. Yee, J. I. Lee, D. M. Park, K. Jung, S. Lee, N. H. Kim, J. Kim, H. J. Kim and M. S. Kang, *Small*, 2024, **20**, e2307190.
75 Y. Hu, Y. He, Z. Peng and Y. Li, *Biosens. Bioelectron.*, 2020, **167**, 112490.
76 Q. Tao, N. Tang, Y. Jiang, B. Chen, Y. Liu, X. Xiong and S. Liu, *Biosens. Bioelectron.*, 2023, **237**, 115452.
77 J. Zhao, C. X. Chen, J. W. Zhu, H. L. Zong, Y. H. Hu and Y. Z. Wang, *Anal. Chem.*, 2022, **94**, 4303–4310.
78 N. Arab, M. Hosseini, G. Xu, N. Sadeghi and H. Rabbani, *Biosens. Bioelectron.*, 2025, **282**, 117482.
79 Y. Z. Wang, Y. Q. Zhang, Y. Liu, Y. R. Li, M. L. Li, G. R. Meng, L. Mi, Y. H. Hu and J. J. Xu, *Anal. Chem.*, 2024, **96**, 5852–5859.
80 Y. Luo, F. Lv, M. Wang, L. Lu, Y. Liu and X. Xiong, *Sens. Actuators, B*, 2021, **349**, 130761.
81 Y. L. Jia, C. H. Xu, X. Q. Li, H. Y. Chen and J. J. Xu, *Anal. Chim. Acta*, 2023, **1251**, 340980.
82 Q. Tao, N. Tang, S. OuYang, Y. Jiang, Y. Luo, Y. Liu and X. Xiong, *Food Anal. Methods*, 2022, **16**, 491–498.
83 E. Kerr, E. H. Doeven, G. J. Barbante, C. F. Hogan, D. J. Bower, P. S. Donnelly, T. U. Connell and P. S. Francis, *Chem. Sci.*, 2015, **6**, 472–479.
84 L. C. Soulsby, E. H. Doeven, T. T. Pham, D. J. Eyckens, L. C. Henderson, B. M. Long, R. M. Guijt and P. S. Francis, *Chem. Commun.*, 2019, **55**, 11474–11477.
85 L. C. Soulsby, D. J. Hayne, E. H. Doeven, D. J. D. Wilson, J. Agugiaro, T. U. Connell, L. Chen, C. F. Hogan, E. Kerr, J. L. Adcock, P. S. Donnelly, J. M. White and P. S. Francis, *Phys. Chem. Chem. Phys.*, 2018, **20**, 18995–19006.
86 W. Gao, K. Muzyka, X. Ma, B. Lou and G. Xu, *Chem. Sci.*, 2018, **9**, 3911–3916.
87 X. Ma, L. Qi, W. Gao, F. Yuan, Y. Xia, B. Lou and G. Xu, *Electrochim. Acta*, 2019, **308**, 20–24.
88 F. Du, Z. Dong, Y. Guan, A. M. Zeid, D. Ma, J. Feng, D. Yang and G. Xu, *Anal. Chem.*, 2022, **94**, 2189–2194.
89 K. Xue, B. Lin, S. Huang, B. Cai, W. Lai, T. Zhan, Y. Liang and C. Zhang, *Sens. Actuators, B*, 2023, **393**, 134259.
90 Y. Liang, K. Xue, Y. Shi, T. Zhan, W. Lai and C. Zhang, *Anal. Chem.*, 2023, **95**, 3434–3441.
91 Y. Su, W. Lai, Y. Liang and C. Zhang, *Anal. Chim. Acta*, 2022, **1206**, 339789.
92 L. Zhu, X. Lv, H. Yu, X. Tan, Y. Rong, W. Feng, L. Zhang, J. Yu and Y. Zhang, *Anal. Chem.*, 2022, **94**, 8327–8334.
93 Y. Hu, L. Zhu, X. Mei, J. Liu, Z. Yao and Y. Li, *Anal. Chem.*, 2021, **93**, 12367–12373.
94 X. Wang, W. Yuan, Z. Sun, F. Liu and D. Wang, *Food Chem.*, 2023, **403**, 134240.
95 S. Wang, X. Li, X. Wang, X. Wu, D. Jiang, H. Zhou, S. Gao and J. Liu, *Biosens. Bioelectron.*, 2024, **253**, 116170.
96 Y. Huang, S. Zhang, Y. Chen, H. Dai and Y. Lin, *Anal. Chem.*, 2022, **94**, 13269–13277.
97 S. Wang, T. Wang, Z. Wang, G. Liu, R. Ji, Y. Zang, S. Lin, J. Lu, H. Zhou and Q. Wang, *Biosens. Bioelectron.*, 2024, **265**, 116704.
98 Y. Wang, R. Jin, N. Sojic, D. Jiang and H. Y. Chen, *Angew. Chem., Int. Ed.*, 2020, **59**, 10416–10420.
99 Y. Wang, D. Jiang and H.-Y. Chen, *CCS Chem.*, 2022, **4**, 2221–2227.
100 T. Iwama, M. Komatsu, K. Y. Inoue and H. Shiku, *ChemElectroChem*, 2021, **8**, 3492–3498.
101 T. Iwama, K. Y. Inoue and H. Shiku, *Anal. Chem.*, 2022, **94**, 8857–8866.
102 T. Iwama, K. Y. Inoue, H. Abe, T. Matsue and H. Shiku, *Analyst*, 2020, **145**, 6895–6900.
103 T. Iwama, Y. Guo, S. Handa, K. Y. Inoue, T. Yoshinobu, F. Sorin and H. Shiku, *Adv. Mater. Technol.*, 2022, **7**, 2101066.
104 K. Hiramoto, E. Villani, T. Iwama, K. Komatsu, S. Inagi, K. Y. Inoue, Y. Nashimoto, K. Ino and H. Shiku, *Micromachines*, 2020, **11**, 530–552.
105 R. Akasaka, K. Ino, T. Iwama, K. Y. Inoue, Y. Nashimoto and H. Shiku, *Sens. Mater.*, 2022, **34**, 3113–3122.
106 G. Li and R. Hao, *Sens. Actuators Rep.*, 2024, **8**, 100220.
107 T. J. Anderson, P. A. Defnet and B. Zhang, *Anal. Chem.*, 2020, **92**, 6748–6755.
108 X. Li, X. Qin, Z. Wang, Y. Wu, K. Wang, X. Xia and S. Liu, *ACS Sens.*, 2022, **7**, 2446–2453.
109 X. Qin, H. J. Jin, X. Li, J. Li, J. B. Pan, K. Wang, S. Liu, J. J. Xu and X. H. Xia, *Chemistry*, 2022, **28**, e202103964.
110 Y. Wang, Q. Lu and D. Huang, *Microchim. Acta*, 2023, **191**, 4.
111 S. Voci, A. Ismail, P. Pham, J. Yu, A. Maziz, F. Mesnilgrente, L. Reynaud, T. Livache, P. Mailley, A. Buhot, T. Leichle, A. Kuhn, L. Leroy, A. Bouchet-Spinelli and N. Sojic, *J. Electrochem. Soc.*, 2020, **167**, 137509.
112 X. Y. Wang, S. T. Wu, Y. Z. Lin, S. N. Ding, J. J. Xu and H. Y. Chen, *Anal. Chem.*, 2024, **96**, 14372–14381.
113 S. M. Beladi-Mousavi, G. Salinas, L. Bouffier, N. Sojic and A. Kuhn, *Chem. Sci.*, 2022, **13**, 14277–14284.
114 Y. Fu, B. Xie, M. Liu, S. Hou, Q. Zhu, A. Kuhn, L. Zhang, W. Yang and N. Sojic, *Chem. Sci.*, 2024, **15**, 19907–19912.
115 A. L. Dauphin, A. Akchach, S. Voci, A. Kuhn, G. Xu, L. Bouffier and N. Sojic, *J. Phys. Chem. Lett.*, 2019, **10**, 5318–5324.
116 V. Eßmann, J. Clausmeyer and W. Schuhmann, *Electrochim. Commun.*, 2017, **75**, 82–85.
117 C. Li, M. Feng, D. Stankovic, L. Bouffier, F. Zhang, Z. Wang and N. Sojic, *Analyst*, 2024, **149**, 2756–2761.
118 L. R. Arias-Aranda, G. Salinas, A. Kuhn, G. Xu, F. Kanoufi, L. Bouffier and N. Sojic, *Chem. Sci.*, 2024, **15**, 8723–8730.
119 E. Villani, N. Shida and S. Inagi, *Electrochim. Acta*, 2021, **389**, 138718.
120 M. Liu, L. R. Arias-Aranda, H. Li, L. Bouffier, A. Kuhn, N. Sojic and G. Salinas, *ChemPhysChem*, 2024, **25**, e202400133.
121 H. Lee, J. Kim, M. Hwang and J. Kim, *ACS Sens.*, 2023, **8**, 4374–4383.
122 M. Liu, G. Salinas, J. Yu, A. Cornet, H. Li, A. Kuhn and N. Sojic, *Chem. Sci.*, 2023, **14**, 10664–10670.